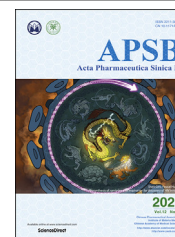Chinese Pharmaceutical Association
Institute of Materia Medica, Chinese Academy of Medical Sciences

Acta Pharmaceutica Sinica B

APSB
Acta Pharmaceutica Sinica B

2022

ORIGINAL ARTICLE

A potent PGK1 antagonist reveals PGK1 regulates the production of IL-1β and IL-6

Liping Liao[b,c,†], Wenzhen Dang[a,b,†], Tingting Lin[b,c,†], Jinghua Yu[b], Tonghai Liu[b,c], Wen Li[b], Senhao Xiao[b,c], Lei Feng[b,c], Jing Huang[b,c], Rong Fu[b], Jiacheng Li[b,c], Liping Liu[b,c], Mingchen Wang[b,c], Hongru Tao[b], Hualiang Jiang[b,c], Kaixian Chen[b,c], Xingxing Diao[b], Bing Zhou[b,d,*], Xiaoyan Shen[a,*], Cheng Luo[a,b,c,d,e,*]

[a]Department of Pharmacology & the Key Laboratory of Smart Drug Delivery, Ministry of Education, School of Pharmacy, Fudan University, Shanghai 201203, China
[b]State Key Laboratory of Drug Research, Shanghai Institute of Materia Medica, Chinese Academy of Sciences, Shanghai 201203, China
[c]University of Chinese Academy of Sciences, Beijing 100049, China
[d]School of Pharmaceutical Science and Technology, Hangzhou Institute for Advanced Study, University of Chinese Academy of Sciences, Hangzhou 310024, China
[e]School of Pharmaceutical Sciences, Zhejiang Chinese Medical University, Hangzhou 310053, China

Abstract Glycolytic metabolism enzymes have been implicated in the immunometabolism field through changes in metabolic status. PGK1 is a catalytic enzyme in the glycolytic pathway. Here, we set up a high-throughput screen platform to identify PGK1 inhibitors. DC-PGKI is an ATP-competitive inhibitor of PGK1 with an affinity of $K_d = 99.08$ nmol/L. DC-PGKI stabilizes PGK1 *in vitro* and *in vivo*, and suppresses both glycolytic activity and the kinase function of PGK1. In addition, DC-PGKI unveils that PGK1 regulates production of IL-1β and IL-6 in LPS-stimulated macrophages. Mechanistically, inhibition of PGK1 with DC-PGKI results in NRF2 (nuclear factor-erythroid factor 2-related factor 2, NFE2L2) accumulation, then NRF2 translocates to the nucleus and binds to the proximity region of *Il-1β* and *Il-6* genes, and inhibits LPS-induced expression of these genes. DC-PGKI ameliorates colitis in the dextran sulfate sodium (DSS)-induced colitis mouse model. These data support PGK1 as a regulator of macrophages and suggest potential utility of PGK1 inhibitors in the treatment of inflammatory bowel disease.

*Corresponding authors.
E-mail addresses: zhoubing@simm.ac.cn (Bing Zhou), shxiaoy@fudan.edu.cn (Xiaoyan Shen), cluo@simm.ac.cn (Cheng Luo).
†These authors made equal contributions to this work.

1. Introduction

Glycolysis is the fundamental energy generation pathway, almost conserved in all kinds of creatures. Aerobics glycolysis has been known as one of the hallmarks of malignant tumors for a century[1–3]. In addition, aerobic glycolysis also has crucial effects on immune cell activation and function[4–6]. The versatile biological roles of aerobic glycolysis are mainly dependent on its metabolic enzymes. Those enzymes possess multiple functions that surpass metabolic processes[7–14].

Phosphoglycerate kinase1 (PGK1, EC 2.7.2.3) is the seventh step catalytic enzyme, responding to the first ATP production in the glycolytic pathway by converting 1,3-bisphosphoglycerate (1,3-BPG) to 3-phosphoglycerate (3-PG). Loads of works have been reported that overexpression or enhanced glycolytic activity of PGK1 correlates with poor tumor prognosis and chemotherapy resistance[15]. For instance, PGK1 is upregulated in ovarian cancer[16,17], breast cancer[18], pancreatic cancer[19,20], and colorectal cancer[21], and PGK1 was found to be assist cell resistance to 5-FU in gastric cancer[22,23]. The regulation of PGK1 is sophisticated. At the transcription level, MYC and HIF1α were well-known to increase glycolytic enzymes in the context of highly aerobic glycolysis through binding to the promoter region of PGK1[24–27]. Contrast, PARRY constraint PGK1 expression[18]. The function of PGK1 is also regulated by various posttranslational modifications, such as acetylation in K220[28,29], K323[30], and K388[31] or phosphorylation in S203[32], S256[33], T243[34], and Y324[35], O-glcnacylation modification in T255[36], which enhance PGK1 glycolytic activity. Aside from its glycolytic activity, PGK1 attracts much attention as a kinase. PGK1 phosphorylates PDHK1 to coordinate cell energy production and maintain the cellular redox environment[5], and phosphorylation of Beclin1 by PGK1 initiates autophagy in the context of nutrient restriction[31].

However, despite the role of PGK1 in tumor proliferation, drugs or compounds designed to target PGK1 remain still few. The reported drug terazosin, an α1-adrenergic receptor antagonist, is approved to treat enlarged prostate. It activates PGK1 to produce more ATP to activate HSP90, thus protecting organ damage from multi-stress challenges[37]. But what remains unclear is whether Terazosin exhibit its organ protective effect on activating PGK1 *in vivo*. Another reported PGK1 inhibitor, CBR-470-1, uncovered the interaction of glycolysis with the NRF2 pathway. CBR-470-1 exerted a cytoprotective effect by inhibiting PGK1 causing the accumulation of upstream metabolites, and then covalently modified KEAP1 to activate NRF2[38]. Both these compounds revealed the novel functions of PGK1 beyond the tumor, indicating that the role of PGK1 is much complex. Hence, we aim to find the novel chemical entities targeting PGK1 and use those chemical probes to explore biological functions of PGK1.

Herein, we first set up a high-throughput screen platform to identify PGK1 inhibitors. Next, with the combination studies of enzymology and chemical optimization, we explored the mechanism of action of the lead compound DC-PGKI (ethyl 6,7-dichloro-3-(4-((4-(piperazin-1-yl)phenyl)carbamoyl) piperazin-1-yl) quinoxaline-2-carboxylate), which is an ATP-competitive inhibitor of PGK1 with a high binding affinity (K_d = 99.08 nmol/L). Additionally, DC-PGKI stabilizes PGK1 *in vitro* and *in vivo*, and suppresses both the glycolytic activity and the kinase function of PGK1. Furthermore, DC-PGKI unveils that PGK1 regulates production of IL-1β and IL-6 in LPS-stimulated macrophages. Mechanistically, inhibition of PGK1 with DC-PGKI results in NRF2 accumulation, which translocates to nucleus and binds to the proximity of *Il-1β* and *Il-6* genes, thus hurdles *Il-1β* and *Il-6* transcription. More importantly, treatment with DC-PGKI attenuates the symptoms of DSS-induce acute colitis mice.

2. Materials and methods

2.1. Reagents

Antibodies to GAPDH (CAT#5174), pro-IL-1β (CAT#12242), pSer30 Beclin1 (CAT#54101), Beclin1 (CAT#3495), IL-6 (CAT#12912), KEAP1 (CAT#8047), NRF2 (CAT#12721), β-tubulin (CAT#2146) were from CST (Signaling Technology, USA). Antibodies to PGK1 (CAT#17811-1-AP), HMOX1 (CAT#10701-1-AP) were from Proteintech (USA). Antibody to Actin were from Sangon Biotech (Shanghai, China). Mouse IL-1β and IL-6 ELISA kits were purchased from Dakewe Biotech Co., Ltd. Dextran sulfate sodium salt (CAT#MB5535) was obtained from Meilunbio (Dalian, China). Dulbecco's modified Eagle medium were obtained from Shanghai BasalMedia Technologies Co., Ltd. (Shanghai, China). Fetal bovine serum (FBS) was obtained from Gibco (Life Tech, Grand Island, NY, USA). Terazosin (CAT#BD41900), dorsomorphin (CAT#BD237195), purvalanol A (CAT#BD149563), MK-571 (CAT#BD244004) were purchased from Bide Pharmatech Ltd. (Shanghai, China). DC-PGKI was synthesized by ourselves. The purity of DC-PGKI was determined by Waters UPLC H-Class with ACQUITY UPLC BEH C18 reversed-phase column (2.1 mm × 50 mm, 1.7 mm) and was confirmed to be more than 95%.

2.2. Cell lines

RAW264.7 cells were cultured in Dulbecco's modified Eagle's medium (10% fetal bovine serum, supplemented with 1% penicillin-streptomycin). NCI-H460 and A549 cells were cultured in RPMI 1640 medium. Cells were tested with the MycoBlue Mycoplasma Detector month. Bone marrow-derived macrophages (BMDMs) were derived from C57BL/6 mice as described previously[39] and cultured in DMEM supplemented with 10% FBS and M-CSF (20 ng/mL) for 7 days.

2.3. Protein expression and purification

The DNA fragment of PGK1 was amplified from the laboratory-constructed human cDNA library (TransFast Taq DNA Polymerase, AP101-01) and subcloned into a linearized pET28a

vector, which was transferred into DH5α competent cells. Monoclonal colonies were picked for Sanger sequencing (Biochemical Bioengineering, Ltd.) and plasmids were extracted for protein expression and purification. The pET28a-PGK1 was transformed into BL21 (DE3) PlysS competent cells (TransGen Biotech), cultured in 1 L Luria–Bertani (LB) medium at 37 °C until the absorbance at OD_{600} was 0.4–0.6 and were induced with 0.4 mmol/L isopropyl-D-thiogalactose (IPTG) for 3 h. Later, the cells were collected by centrifugation at 4000 rpm for 15 min and were stored at −80 °C. The pellets were resuspended and lysed with cell lysates (20 mmol/L HEPES pH 7.4, 200 mmol/L NaCl, 4 mmol/L β-mercaptoethanol). The cell supernatant flowed through an equilibrated nickel column at 0.8 mL/min (GE Healthcare). Buffer A (20 mmol/L HEPES pH 7.4; 200 mmol/L NaCl; 4 mmol/L β-ME; 20 mmol/L imidazole) was used to eliminate unspecific binding protein. Then PGK1 protein was eluted with a gradient mix of buffer A with buffer B (20 mmol/L HEPES pH 7.4; 200 mmol/L NaCl; 4 mmol/L ME; 1 mol/L imidazole) in the AKTA system (GE Healthcare). The purified protein was analyzed by SDS-PAGE electrophoresis to determine the protein size and purity. Protein fractions with greater than 90% purity were passed by desalting columns (GE Healthcare) under desalination buffer (20 mmol/L HEPES pH 7.4, 200 mmol/L NaCl). For other assays, PGK1 was supplemented with 20% glycerol frozen for subsequent experiments. For crystallization, His-PGK1 was cleaved by TEV at 4 °C overnight. Further purified *via* nickel column and molecular gel exclusion chromatography (Superdex 75 increase GE Healthcare) with buffer system (50 mmol/L Tris-HCl pH 7.4, 150 mmol/L NaCl), high concentration protein components were collected for crystallization experiments, the remaining proteins were packed with 20% glycerol nitrogen and flash frozen in the −80 °C refrigerator.

2.4. Steady-state kinetic assay

The catalytic activity of the PGK1 was determined using a PGK1 and GAPDH-coupled enzyme active system. The initiate velocity (V_0) was defined as less than 10% ATP has been consumed in the enzymatic reaction. Thus, we calculate the V_0 at the first 3 min of reaction when the substrate concentration is not the limiting factor of the reaction. All V_0 was determined in the same manner. The buffer system (100 mmol/L Tris-HCl, 150 mmol/L NaCl, 0.5 mmol/L EDTA, 2 mmol/L MgCl$_2$, 1 mmol/L DTT, 1 mg/mL BSA) was subject to all enzymatic assay system. To characterize the enzymatic activity of our recombinant PGK1. We determined the kinetic parameters through the steady-state kinetic assay. We first determined the appropriate concentration of PGK1. Gradient concentrations of PGK1 were added to the reaction system (6 mmol/L 3-PG, 2.5 mmol/L ATP, 250 μmol/L NADH, 0.1 μmol/L GAPDH) to initiate the reaction, then calculated the V_0 of each concentration of PGK1, and plotted in Supporting Information Fig. S1D. Thus, we decided to use 0.4 nmol/L of PGK1 and 0.1 μmol/L GAPDH as our assay enzymes' fractions, and all enzymatic assay was done in the same enzyme concentration of PGK1 and GAPDH. The K_m values of 3-PG were determined with 3 mmol/L ATP, 250 μmol/L NADH, 3-PG concentrations ranging from 0 to 9 mmol/L. The K_m values of ATP were determined with 6 mmol/L 3-PG, 250 μmol/L NADH, ATP concentration ranging from 0 to 9 mmol/L. The data were globally fitted in the Michaelis−Menten equation in the Graphpad Prism 7.0.

When it comes to determining the apparent V_{max} and K_m in the presence of gradient compound concentrations, the 3-PG range from 0 to 4 mmol/L with the fixed 6 mmol/L of ATP and the same enzymes fraction as above described. While the apparent K_m of ATP was determined under fixed 4 mmol/L 3-PG and ATP range 0−18 mmol/L. The data of 3-PG were globally fitted in the non-competitive model, while the ATP data were globally fitted in the competitive model by Graphpad Prism 7.0.

2.5. High-throughput screening

The total 100 μL high-throughput assay system contained three fractions: 50 μL of 2 × substrate section (final concentration: 2 mmol/L of 1,3-BPG, 1.5 mmol/L of ATP, 200 μmol/L of NADH), 49 μL 2 × the enzymes fraction (final concentration: 0.4 nmol/L PGK1 and 0.1 μmol/L GAPDH), and 1 μL compound fraction (final concentration: 50 μmol/L). All fraction was in the assay buffering reagent (100 mmol/L Tris-HCl, 150 mmol/L NaCl, 0.5 mmol/L EDTA, 2 mmol/L MgCl$_2$, 1 mmol/L DTT, 1 mg/mL BSA), expect compounds were in the DMSO solution. First, the enzyme fraction was incubated with the compound fraction for 5 min, and then the substrate fraction was added to initiate the reaction and mixed, and immediately monitor OD_{340} nm in the spectrometer machine (ThermoFisher) for 15 min. The initiate velocity (V_0) was defined as less than 10% ATP has been consumed in the enzymatic reaction. Thus, we calculate the V_0 at the first 3min of reaction when the substrate concentration is not the limiting factor of the reaction. Z′-factor of the HTS determined by detecting many wells of positive compound signal (100 μmol/L Terazosin) and the negative compound signal (1% of DMSO), then the Z′-factor is determined by Zhang's method[40].

2.6. IC$_{50}$ determination of hit compound

99 μL 0.4 nmol/L PGK1 was added to a 96-well plate with 1 μL of different concentrations of compounds added. At room temperature, the plate was incubated at 400 rpm for 10 min. 100 μL of the reaction buffer (1.5 mmol/L ATP, 2 mmol/L 3-PG, 200 μmol/L NADH, 0.1 μmol/L GAPDH) was distributed into wells. The absorbance of OD_{340} nm was then measured at 37 °C, and the reading interval was 15 s for 15 min using the kinetic mode of the instrument. The inhibition rate was calculated as Eq. (1):

Compound inhibition rate (%) = (Initial velocity of DMSO−initial velocity of the compound)/Initial velocity of DMSO × 100 (1)

2.7. Protein thermal shift assay

Protein thermal shift assay was used to characterize whether small molecules can affect protein thermal stability. The assay buffer consists of 50 mmol/L HEPES pH 7.4,150 mmol/L NaCl and 1 mmol/L DTT. The total volume is 20 μL, including 3 μmol/L PGK1 protein, 5 × SYPRO orange dye, 0.5 μL compound or DMSO. QuantStudio™ 6 Flex Real-Time PCR System (Applied Biosystems) instrument was subject to detect the signal, and data were calculated with the built-in protein thermal shift software, then were replot by Graphpad prism7.0.

2.8. Cellular thermal shift assay

As for the fixed heating temperature group, RAW264.7 cells (5×10^5 cells) were seeded in 12-well plates, after overnight adherent, corresponding concentrations of DC-PGKI compound were added in culture medium and treated cells for 3 h. Cells were collected and washed by PBS twice to remove the remaining compound. Then cells were suspended with 220 μL PBS containing $1 \times$ protease inhibitor. 60 μL cell suspension was treated as the reference without heating. The remnant was heated in the PCR instrument at 52 °C for 3 min, then frozen with liquid nitrogen and thawed in 25 °C water twice. Cell lysates were centrifuged at 4 °C, $20,000 \times g$ for 20 min. Cell supernatant was transferred into a new EP tube and added a corresponding volume of $6 \times$ SDS loading samples for Western blot. 1.5×10^6 cells were plated in each 6 cm dish of three dishes after the overnight adherent. The cells were treated with DMSO, 20 or 5 μmol/L PGK1 for 3 h, respectively. Then the harvested cells of each group were divided into eight tubes, respectively. Each tube of corresponding treatment was subject to heat at eight different temperatures for 3 min in a Bio-Rad PCR machine and lysis, followed by the process described above.

2.9. Glucose and lactate level determination

RAW264.7 cells (1×10^6) were seeded in 6-well plates overnight. After washed three times with PBS, the cells were treated with culture medium (10% dialyzed FBS (Gibco), 20 mmol/L glucose solution (Aligent), and glucose-free DMEM medium) and the corresponding concentrations of compounds for 10 h. RAW264.7 cells were stimulated with 1 μg/mL LPS for 4 h. Cell supernatant was harvested to determine the glucose content and lactate content. Glucose was determined by hexose kinase and glucose-6-phosphate dehydrogenase coupling assay. First, glucose was phosphorylated by hexose kinase, after which glucose 6-phosphate and $NADP^+$ converted to gluconate-1,5-lactone-6-phosphate and NADPH. The content of NADPH was determined based on NADPH absorption at 340 nm. The glucose consumed was calculated from the total glucose content minus the remaining glucose content in the medium. Lactate was determined by the lactate dehydrogenase method. In the presence of NAD^+, lactate is converted to lactate pyruvate by dehydrogenase while generating NADH. Thus we can calculate the lactate content in the medium. Both the glucose consumption and lactate production were normalized to the cell number.

2.10. Small interfering RNA transfection assay

RAW264.7 (2×10^6) cells with 200 nmol/L siRNA were subject to electroporation by using the Lonza VCA-1003 assay kit. PGK1 siRNAs designed by GenePharma were transferred into cells with Lonza 2b according to the manufacturer's recommended procedure. 12 h later, the cells were divided into two parts, one was used to detect knockdown efficiency, and the other was used to observe the effect of PGK1siRNA on inflammatory factors. The PCDNA3.1-3flag-mPGK1 plasmid was synthesized with synonymous substitution, resistant to both independent siRNA (Shanghai Generay Biotech Co., Ltd.). The rescue assay was also done by the same Nucleofector kit and the PCDNA3.1-GFP vector as the control.

2.11. ELISA

RAW264.7 cells were pre-treated with compounds for 3 h and then with or without additional 1 μg/mL LPS for another 4 h. The culture medium was collected to measure the concentration of TNFα using the TNFα ELISA kit (Abcam, ab181421) according to the manufacturer's instructions.

2.12. Western blotting

RAW264.7 cells (1.5×10^6) or BMDM cell were seeded into 6-well plates and incubated overnight. After pretreatment with the indicated concentrations of compounds for 3 h, cells were stimulated with or without additional 1 μg/mL LPS for another 4 h. H460 (5×10^5) or A549 cell were seeded into 12-well plates and attached overnight. Cells were treated with the indicated concentrations of compounds for 8 h. RIPA buffer supplemented with protease/phosphatase inhibitor tablets was used to lyse cells. Protein concentrations in the lysates were quantified by BCA assay (ThermoFisher), then diluted with $6 \times$ SDS buffer and denatured for 10 min at 100 °C. Samples (15−30 μg) of total proteins were separated via SDS-PAGE and transferred to a nitrocellulose membrane, which was blocked for 1 h at room temperature in the TBST buffer containing 5% milk and was incubated with the primary antibody overnight at 4 °C. After washing, the membrane was incubated with HRP-conjugated secondary antibody (1:10,000) for 1 h in 5% milk at RT and then treated with ECL Western Blotting Substrate (ThermoFisher) and visualized.

2.13. qRT-PCR

Total RNA was extracted from cells with RNA isolater Total RNA Extraction Reagent (Vazyme Biotech) according to the manufacture's instruction. HiScript Q RT SuperMix kit (Vazyme Biotech) was used for the reverse transcription with 1 μg of total RNA. ChamQ SYBR qPCR master mix (Vazyme Biotech) was applied to perform qRT-PCR using a Quant Studio 6 Flex real-time PCR system (Applied Biosystems). Sequences of primers are listed in Supporting Information Table S1.

2.14. ChIP-qPCR

ChIP-qPCR was performed according to the following steps[41,42]. RAW264.7 cells were collected and resuspended in 10 mL PBS, and 278 μL of 37% formaldehyde was added to a final concentration of 1% for cross-linking at room temperature for 10 min. 541 μL of 2.5 mol/L glycine was added to terminate the cross-linking reaction for 5 min. After centrifugation at $2500 \times g$ for 5 min, the cell pellets were washed with 5 mL PBS containing $1 \times$ protease inhibitor and then lysed cell membrane in Pre-Lysis Buffer (10 mmol/L Tris-HCl pH 8.0, 10 mmol/L NaCl, 0.2% NP-40, and $1 \times$ proteinase inhibitor) for 30 min at 4 °C. The samples were centrifuged at $2500 \times g$ for 5 min at 4 °C, and 500 μL Pre-Lysis Buffer washed the pellets. Cells were resuspended by Nuclear Lysis Buffer (50 mmol/L Tris-HCl pH 7.5, 10 mmol/L EDTA, 1% SDS, and $1 \times$ proteinase inhibitor) and sheared in Nuclear Lysis Buffer using Covaris S220 Ultrasonic crusher. The samples were then centrifuged at $15,000 \times g$ for 15 min at 4 °C, and the supernatants were carefully transferred to new tubes. 5% of the samples were saved as ChIP input controls. After preclearing using 30 μL of protein G beads (Invitrogen). 5 μL of

anti-NRF2 antibody was added (CST) for immunoprecipitation overnight. 50 μL of protein G beads were incubated with rotation for 3 h at 4 °C. The protein G beads were washed twice each with Low Salt Wash Buffer (0.1% SDS, 1% Triton X-100, 2 mmol/L EDTA, 20 mmol/L Tris-HCl, 150 mmol/L NaCl), High Salt Wash Buffer (0.1% SDS, 1% Triton X-100, 2 mmol/L EDTA, 20 mmol/L Tris-HCl, 500 mmol/L NaCl), and LiCl Wash Buffer (10 mmol/L Tris pH 7.5, 250 mmol/L LiCl, 1% NP-40, 1% Na-Doc, 1 mmol/L EDTA) and resuspended in 100 μL of freshly DNA Elution Buffer (50 mmol/L $NaHCO_3$ and 1% SDS). The ChIP sample beads were placed on a magnet, and the supernatant was transferred to a new tube. The samples were digested with 10 μL of Proteinase K (Invitrogen, 25530049) and then incubated at 65 °C for 4 h. DNA was purified with DNA Clean & Concentrator-5 (Zymo Research, D4004). 0.5 μL of eluted DNA was performed to the template for ChIP-qPCR with SYBR qPCR Mix according to the manufacturer's protocol. The primer sequences used for ChIP-qPCR were referred to the paper[42].

2.15. In vivo pharmacokinetic study

The pharmacokinetic assay of DC-PGKI were performed in male mice. The male mice were administered orally (po) or intravenously (iv) at a dose of 10 and 3 mg/kg DC-PGKI separately. Then, blood samples were collected into tubes containing EDTA at 0.25, 0.5, 1, 2, 4, 6, 8, 24 h (po) and 0.083, 0.25, 0.5, 1, 2, 4, 8, 24 h (iv) after dosing. After centrifugation at 6000 rpm for 10 min at 4 °C, the obtained plasma samples were stored at −20 °C. Subsequently, the plasma samples were analyzed by liquid chromatography−tandem mass spectrometry (LC−MS/MS) analysis.

2.16. Animal experiments

The 8-week-old C57BL/6 male mice were randomly divided into five groups. The normal group and the model group were intraperitoneal injection with 10% (v/v) DMSO in sterile-filtered PBS, and DC-PGKI group were intraperitoneal injection with DC-PGKI prepared with 10% DMSO+90% PBS (10 mg/kg/day and 5 mg/kg/day). The positive group were given the drug mesalazine (5-ASA, 50 mg/kg/day) by gavage. Except for the normal group, mice were given 5% (w/v) DSS for 7 days to induce acute colitis, followed by drink water for one day. Mice were weighed and scored for disease activity index (DAI) daily. DAI was assessed with semi-quantitate the severity of diarrhea and bloody stools[43]. After the mice were euthanized, colon tissue was collected for H&E staining. The levels of IL-6 and IL-β in the serum of each group mice were detected by ELISA kit according to the manufacturer's protocols. The total mRNA and protein were extracted from the same part of mouse colon tissue. The pathological changes in mice were conducted semi-quantitatively under the blind method[44]. All animal experiments were performed according to protocols approved by the Animal Ethics Committee of the Shanghai Institute of Materia Medica, Chinese Academy of Science (Shanghai, China).

2.17. Statistical analysis

All results were presented as mean ± SEM representing three independent experiments. The statistical analyses were performed using GraphPad Prism 7.0. A two-tailed Student's t-test assessed statistical significance between the two groups. The significance level was shown at $^*P < 0.05$, $^{**}P < 0.01$, $^{***}P < 0.001$, $^{****}P < 0.0001$.

3. Results

3.1. Development of a high-throughput screening assay to identify inhibitors of PGK1

To identify inhibitors of PGK1, we set up a high-throughput screen platform based on the PGK1 and GAPDH coupled catalytic process. Physiologically, PGK1 catalyzes 1,3-BPG, the production of GAPDH, to 3-PG with the generation of ATP, the change of Gibbs free energy (ΔG) of this equation is favorable[45], but there is no product for the assay's readout. Fortunately, both GAPDH and PGK1 catalytic processions are reversible. Thus, we decided to determine PGK1 catalytic activity in the reverse reaction coupled with GAPDH. The reaction system contains 3-PG, ATP, NADH, and GAPDH. Then added PGK1 to initiate the reaction, and the excessive GAPDH will immediately convert 1,3-BPG and NADH to GAP, NAD^+ (Fig. 1A, upper panel). Consequently, we can determine the initial rate of PGK1 by calculating NADH consumption through monitoring OD_{340} nm absorbance.

To establish a high-throughput screening (HTS) assay for PGK1, we characterized the kinetic parameters of the recombinant PGK1 purified from the *Escherichia coli* expression system with high purity. The K_m value for 1,3-BPG is 189.4 ± 4.8 μmol/L (Supporting Information Fig. S1A), and the K_m value for ATP is 1.30 ± 0.11 mmol/L (Fig. S1B), and K_{cat} is 956 ± 41.7 s^{-1} (Fig. S1C), similar to the reported human PGK1 data[46]. Then the assay substrates concentration was set as 2 mmol/L of 1,3-BPG and 1.5 mmol/L of ATP and 200 μmol/L of NADH[47]. Next, we optimized the amount and ratio of PGK1 and GAPDH since the assay needs an excessive amount of GAPDH. We set gradient concentrations of PGK1 under a fixed 0.1 μmol/L of GAPDH and then determined the initial rate of PGK1. By plotting the initial velocity as a function of PGK1 at varying concentrations indicated that when the molar ratio of PGK1 to GAPDH reaches 1:200, GAPDH was not enough to immediately convert the 1,3-BPG (Fig. S1D). Thereby we set the concentrations of PGK1 to 0.40 nmol/L and GAPDH to 0.10 μmol/L.

Next, we determined the IC_{50} (half-maximal inhibitory concentration) of terazosin, which is a positive compound in our assay. The Z-factor of our HTS were determined to be 0.54 (Fig. 1B), suggesting that the HTS assay could be applied to screening small molecules on a larger scale. Finally, the HTS assay was subject to screen our in-house compound library. Briefly, a single dose at 50 μmol/L was tested in the primary screen. Only the inhibition rate over 50% was selected for the dose−response curve determination, and those without dose-dependent inhibitory manner and possessed intrinsic absorbance in 340 nm were ruled out. Also, we performed GAPDH catalytic assay (Fig. 1A, lower panel)[47], to remove compounds that interference with GAPDH activity. Eventually, we identified dorsomorphin, purvalanol A, MK-571, and LTP-10 show an apparent inhibition to PGK1 with IC_{50} values of 6.72, 1.96, 25.24 and 2.30 μmol/L (Fig. 1C−D and Figs. S1F−H), respectively.

Among this positive hit compound, purvalanol A exhibits the highest potency against PGK1. Purvalanol A (also named NG52) has been reported as a PGK1 inhibitor with IC_{50} values of 2.5 μmol/L[48], close to our measurement data, indicating that our assay is robust enough to identify PGK1 inhibitors and determine
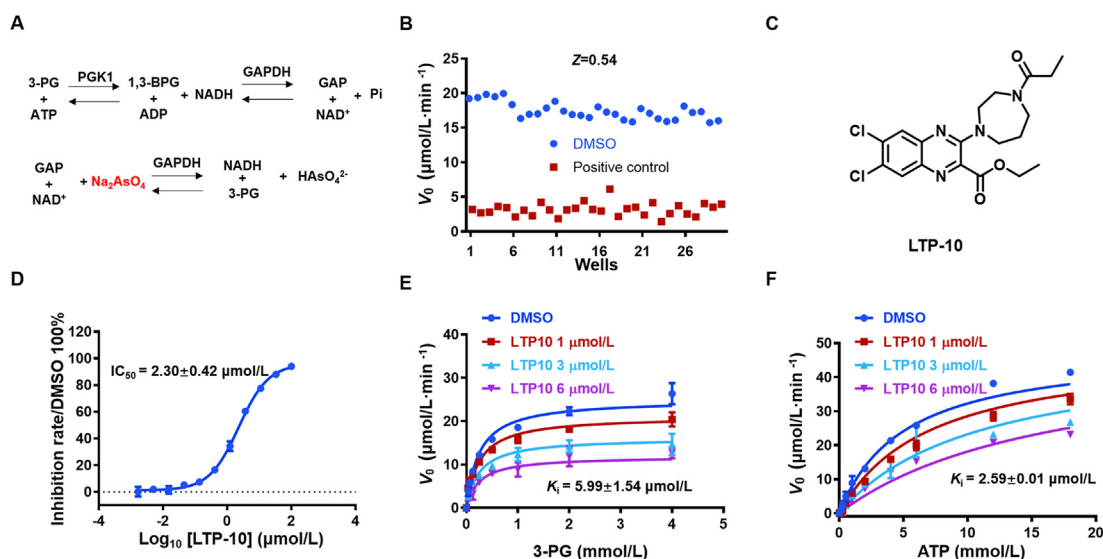
Figure 1 High-throughput assay identified LTP-10 as PGK1 inhibitor. (A) Schematic of PGK1 and GAPDH coupled assay. The product (1,3-BPG) of PGK1 serves as the substrate of GAPDH then the NADH will be consumed. (B) Z-factor (Evaluating parameter of the high-throughput screening assay quality) is determined as Ref. 40. (C) Chemical structure of LTP-10. (D) The IC_{50} of LTP-10 was determined. (E) LTP-10 is a non-competitive with 3-PG.(F) LTP-10 is an ATP competitive inhibitor ($K_i = 2.59 \pm 0.01$ μmol/L). Each data point represents the mean of three independent experiments.

their inhibition potency. LTP-10 ranked in the top two powerful hits with a new chemical scaffold (Fig. 1C). Thus, we decided to choose LTP-10 for further validation. First of all, we performed the enzyme kinetics assay to investigate how LTP-10 inhibits PGK1. As shown in Fig. 1E, LTP-10 decreases V_{max} of 3-PG, while no impact on the K_m of 3-PG, suggesting LTP-10 displays noncompetitive inhibition towards 3-PG, implying that LTP-10 does not interfere with the binding of 3-PG and PGK1. While, LTP-10 increases the K_m of ATP with no apparent change of V_{max}, indicating that LTP-10 competes with ATP, demonstrating that LTP-10 is an ATP competitive inhibitor of PGK1 with the K_i value of 2.59 ± 0.01 μmol/L (Fig. 1F). Next, we assessed whether LTP-10 could increase PGK1 thermal stability similar to terazosin in the protein thermal shift assay. As expected, LTP-10 stabilized PGK1 thermal stability (Figs. S1I−J).

3.2. Development of DC-PGKI as an improved inhibitor

To get further insight into the interaction of LTP-10 with PGK1, we docked LTP-10 to the ADP-binding pocket of PGK1 (PDB ID: 2XE7) (Supporting Information Fig. S2A). The docking predicted that the 6,7-dichloroquinoxaline skeleton of LTP-10 overlapped with the purine ring of the ADP and undergoes halogen-bonding with the surrounding residue (Leu256). 2-carbonyl also formed a hydrogen bond with Glu343 (Fig. S2B). Therefore, we optimized the activity of compounds by modifying the 3-position of quinoxaline, the designed and synthesized multiple analogs (Supporting Information Table S2). In order to reduce the conflict between homopiperazinyl of LTP-10 and the surrounding negatively charged area, we replaced it with piperazinyl (DC-P1, Table S2, $IC_{50} = 0.68 \pm 0.14$ μmol/L). Then we replaced propenyl with other groups, and introduced the aryl to induce π−π interaction with Phe291. Next, we replaced propenyl with uramido and introduced 4-fluorophenyl on uramido moiety (DC-P3, Table S2, $IC_{50} = 0.32 \pm 0.06$ μmol/L). To induce hydrogen bond with Thr254, we replaced fluorine with hydrophilic group. Compound

with 4-piperidyl significantly increased PGK1 inhibitory ability (DC-PGKI, Fig. 2B; $IC_{50} = 0.16 \pm 0.01$ μmol/L).

Next, we conducted substrate titration assays to determine the steady-state constants of PGK1 in the presence of gradient concentrations of DC-PGKI. Under the saturating ATP concentrations, V_{max}'s value of 3-PG decreases with the increase of DC-PGKI, while the apparent K_m is constant, indicating that DC-PGKI is a noncompetitive inhibitor *versus* 3-PG, with the apparent $K_i = 155 \pm 6.00$ nmol/L (Fig. 2C). Under saturating 3-PG concentrations, the value of V_{max} is stable, but the apparent values of K_m increase with the increasing DC-PGKI concentration, suggesting that DC-PGKI is competing with ATP with a K_i of 0.06 ± 0.019 μmol/L (Fig. 2D). Thus, we conclude that DC-PGKI is an ATP-competitive inhibitor of PGK1.

Next, the protein thermal shift assay showed that 15 μmol/L of DC-PGKI increases the melting temperature (T_m) of PGK1 by 4.61 °C (Fig. 2E). To get a specific binding affinity of DC-PGKI to PKG1, we conducted the microscale thermophoresis assay to determine their binding affinity and yielded a K_d of 99.08 nmol/L (Fig. 2F). These data suggest that DC-PGKI directly bind to PGK1.

3.3. DC-PGKI engages PGK1 in cells

Cellular thermal shift assay was subject to address whether DC-PGKI reaches and acts on PGK1 within the cell and at what concentration regimes DC-PGKI exert its effects. Firstly, RAW264.7 cells were treated with varying doses of DC-PGKI for 3 h, and harvested cell to heat at 52 °C, then lysed cell, collected the soluble protein and subsequently subjected to anti-PGK1 Western blotting. DC-PGKI can increase cellular PGK1 thermal stability in a concentration-dependent manner (Fig. 3A). Next, RAW264.7 cells were incubated with 5 or 20 μmol/L DC-PGKI or DMSO for 3 h, then we harvested these group cells and divided into eight tubes equally, respectively. Then the protein samples were heated at varying temperatures and collected the soluble protein, and subjected to anti-PGK1 Western blotting. As
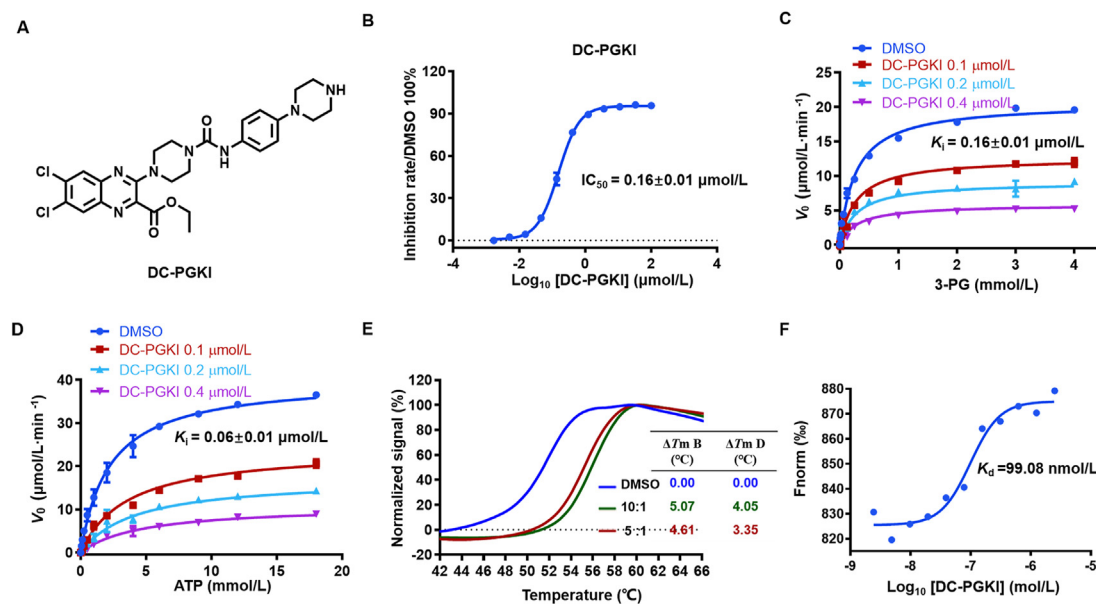
Figure 2 Development of DC-PGKI as an improved inhibitor of PGK1. (A) Chemical structure of DC-PGKI. (B) IC_{50} of DC-PGKI. (C) and (D) Apparent kinetic parameters measured in the absence of DC-PGKI or the presence of the indicated concentrations of DC-PGKI. (E) DC-PGKI is capable of increasing PGK1 thermal stability in protein thermal shift assay. (F) DC-PGKI binds to PGK1 with K_d = 99.08 nmol/L, determined by microscale thermophoresis assay. Each data point represents the mean of three replications in an independent determination with standard errors indicated.

indicated in Fig. 3B, DC-PGKI assists PGK1 resistance to the increasing temperature. Taken together, DC-PGKI is able to permeate the cell membrane and exert the same effect as in the purified protein thermal shift assay in the concentration low to 5 μmol/L.

The glycolytic metabolic enzyme is the fundamental function of PGK1, and macrophages will undergo a metabolism state switch to enhance glycolysis after activation[49,50]. Thus, we evaluated the DC-PGKI effect on PGK1 glycolytic catalysis activity in RAW264.7 cells. In the resting status, 5 μmol/L DC-PGKI significantly suppresses glucose consumption with no apparent impact on the generation of lactates (Fig. 3C and D). In contrast, upon stimulation by LPS, both glucose consumption and lactate production are reduced in the presence of 5 μmol/L DC-PGKI (Fig. 3C and D). But 10 μmol/L DC-PGKI strongly represses the glycolytic pathway in either stimulated or unstimulated macrophages, demonstrating that DC-PGKI inhibits PGK1 glycolytic metabolic activity in the resting and activated macrophage.

We next studied the DC-PGKI effect on PGK1 kinase function by detecting the phosphorylation level of Ser30 Beclin1 under the LPS-challenged macrophage. DC-PGKI notably decreases the Ser30 phosphorylation level of Beclin1 in RAW246.7 cells (Fig. 3E) and bone marrow derived macrophages (BMDM) (Supporting Information Fig. S3C), indicating that DC-PGKI also impairs PGK1's kinase function. Collectively, DC-PGKI significantly suppress the glycolytic catalytic and kinase process of PGK1. These data support that the use of DC-PGKI as a chemical probe that engages PGK1.

3.4. DC-PGKI suppresses LPS-induced macrophage IL-1β and IL-6 production by inhibiting PGK1

Metabolism reprogramming or metabolism switches have been implicated in the immune system—especially aerobic glycolysis in the innate and adaptive immune cells[27,49,51]. PKM2, which has

many commons on PGK1, acts as a kinase that phosphorylates STAT3 to enhance IL-1β and IL-6 expression[52] and phosphorylates EIF2AK2 to activate NLRP3 inflammasome to mature IL-1β[14]. Additionally, TEPP-46 and DASA-58[53] targeted to PKM2 exert anti-inflammation in the animal models of sepsis and encephalomyelitis (EAE)[13,54], implying that targeting glycolytic enzyme may have therapeutic effect on auto-immune diseases.

Given the hints from PKM2 function, we speculate whether PGK1 has a similar manner in regulating pro-inflammation production. Thus, we used DC-PGKI as the chemical tool to study the function of PGK1 in macrophage. DC-PGKI inhibits LPS-induced Il-1β (Fig. 4A) and Il-6 mRNA (Fig. 4B) in a concentration-dependent manner. Tnfα mRNA was upregulated, compared to LPS treatment alone (Fig. S3A). Then we performed Western blot to detect the LPS-induced protein level of pro-IL-1β. DC-PGKI significantly inhibits LPS-induced precursor of IL-1β in RAW264.7 cells as well as BMDM (Fig. 4C and Fig. S3D). Consistently, the Western blot assay indicated that DC-PGKI significantly reduces IL-6 production (Fig. 4C and Fig. S3D). In contrast, the ELISA assay of TNFα showed that DC-PGKI does not affect TNFα secretion (Fig. S3B). The previous studies have revealed that 2-DG blocks LPS-induced IL-1β, while the transcription of IL-6 and TNFα is unaffected[13,55]. Compared to TEPP-46 and DASA-58 only inhibit IL-1β production, DC-PGKI inhibits both IL-1β and IL-6, implying that DC-PGKI may affect other signal pathways to inhibit pro-inflammatory cytokines, in addition to inhibition of glycolytic function.

To investigate the mechanism of DC-PGKI inhibiting LPS-activated IL-1β and IL-6 production, we evaluate whether the effect of DC-PGKI on pro-inflammatory cytokines depends on PGK1. We knocked down PGK1 by two independent small interfering RNA (Fig. 4D and Supporting Information Fig. S4A). In agreement with the inhibitory effect of DC-PGKI, knockdown of PGK1 results in suppression of IL-1β (Fig. 4E and G) and IL-6 (Fig. 4F and G). Knockdown of PGK1 does not affect TNFα
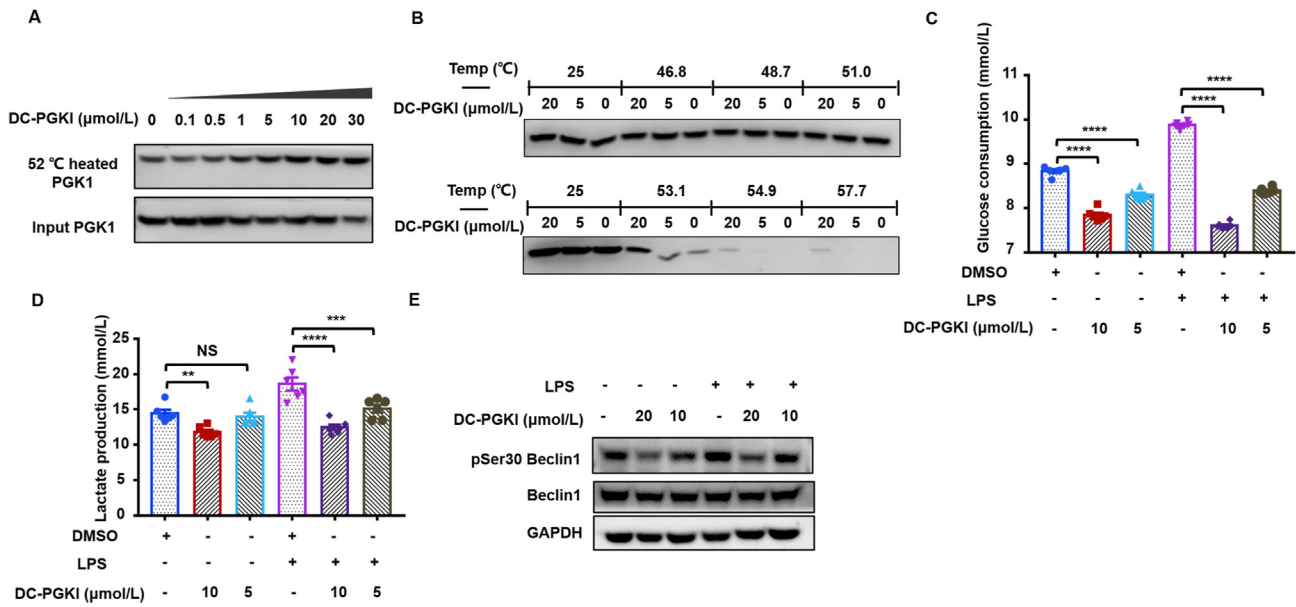
Figure 3 Cellular PGK1 target engagement with DC-PGKI. (A) and (B) RAW264.7 cells were treated with indicated doses of DC-PGKI for 3 h then harvested to the cellular thermal shift assay. (A) All samples were heated at 52 °C, and (B) samples were heated at gradient temperature as indicated. (C) and (D) DC-PGKI suppresses the glycolytic pathway in a PGK1-dependent manner. With or without LPS stimulation, DC-PGKI inhibits the glucose consumption (C) and lactate production (D) of RAW264.7 cells. Data represent mean ± SEM, and each data point represents an independent assay ($n = 6$). Statistical significance were determined by unpaired two-tailed Student's t-test by compared two groups: *$P < 0.05$, **$P < 0.01$, ***$P < 0.001$, ****$P < 0.0001$. (E) DC-PGKI inhibits PGK1 protein kinase function by the inhibition of Ser30 phosphorylation of Beclin1.
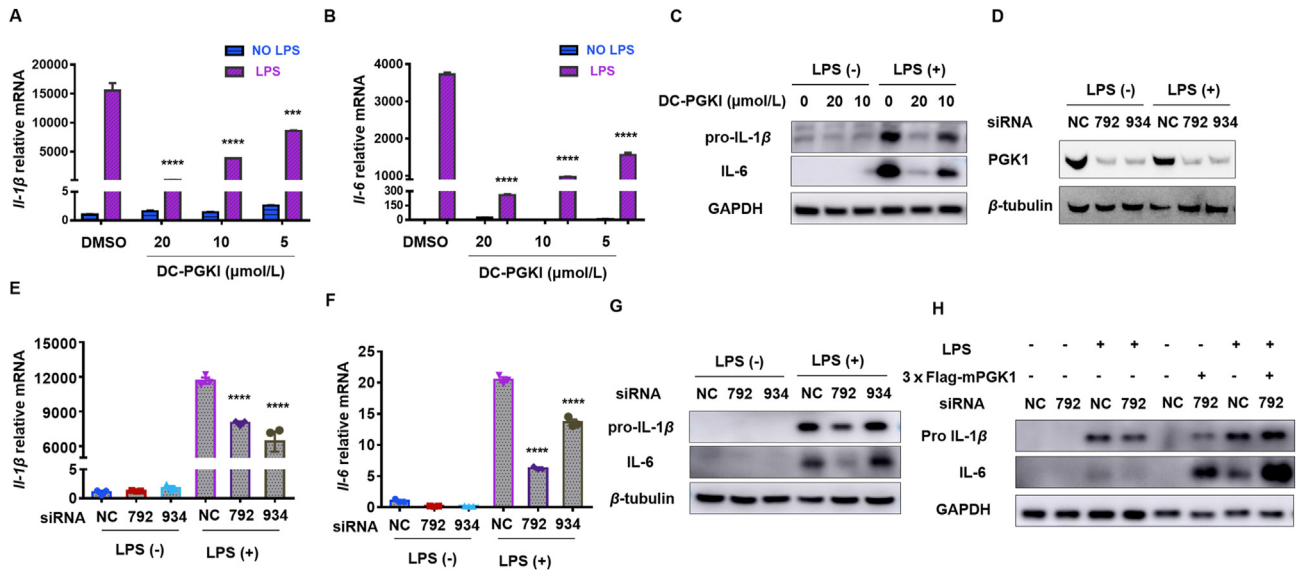

Figure 4 DC-PGKI inhibits LPS-induced macrophage IL-1β, IL-6 production by inhibiting PGK1. (A) and (B) DC-PGKI significantly suppresses the mRNA level of *Il-1β* (A) and *Il-6* (B) at 5 μmol/L. Data represented as mean ± SEM ($n = 3$). Statistical significance was determined by unpaired two-tailed Student's t-test by compared to the LPS-stimulated vehicle control group. *$P < 0.05$, **$P < 0.01$, ***$P < 0.001$, ****$P < 0.0001$. (C) Immunoblot assay indicated that DC-PGKI could dramatically reduce the pro-IL-1β and IL-6 levels. (D) Two siRNA could significantly knockdown of PGK1 on the protein level either in the presence or absence of LPS-challenged RAW264.7 cells. RAW264.7 cells were transfected by using the Lonza nucleofector kit (Cat. VCA-1003). Cells were harvested after 24 h transfection. (E)−(G) Knockdown of PGK1 results in decreasing of *Il-1β* (E) and *Il-6* (F) transcription level as well as the protein level of pro-IL-1β and IL-6 (G). Data represented as mean ± SEM ($n = 3$). Statistical significance was determined by unpaired two-tailed Student's t-test, compared to the LPS-stimulated vehicle control group. *$P < 0.05$, **$P < 0.01$, ***$P < 0.001$, ****$P < 0.0001$. (H) The downregulation of pro-IL-1β and IL-6 by knockdown of PGK1 can be effectively rescued by overexpression of 3×Flag-mPGK1. siRNA transfection and 3×Flag-mPGK1 rescue were done by using Lonza nucleofector kit (Cat. VCA-1003).

expression (Fig. S4B), which is consistent with the 2-DG[56] and TEPP 46[13] treatment.

We next rescued the PGK1 protein level in the siRNA knockdown RAW264.7 cells with the siRNA-resistant 3 × flag-mPGK1 plasmid (Fig. S4C). The decreased production of IL-1β and IL-6 in the siPGK1-KD cell (lane 4) could be rescued by overexpression of PGK1 (lane 8, Fig. 4H). These data demonstrate that the inhibitory effect of DC-PGKI on the production of pro-inflammatory cytokines is dependent on PGK1.

3.5. DC-PGKI promotes NRF2 accumulation to repress IL-1β and IL-6 production

The previous study has showed that the inhibition of PGK1 could result in posttranslational modification of KEAP1[38], which increases NRF2 accumulation and initiates the transcription of various antioxidant genes. In addition, the endogenous metabolite-itaconate[57] exerts its anti-inflammation function through activating NRF2 via alkylate KEAP1[58].

Therefore, we next evaluated whether DC-PGKI could activate NRF2. Incubated with 10 μmol/L DC-PGKI at various times declined the mono-KEAP1 protein level (Supporting Information Fig. S5A) and boosted the NRF2 expression (Fig. S5B), as well as increased the expression of NRF2-responsive gene HMOX1 as early as 7 h (Fig. S5B). RAW264.7 cells were pre-treated various concentrations of DC-PGKI for 3 h then primed macrophage with LPS for another 4 h also resulted in a significant decrease of KEAP1 protein level (Fig. 5A), accumulating NRF2 (Fig. 5B), and increasing both mRNA and protein level of HMOX1 (Fig. 5B and C). Other downstream target genes of NRF2, such as the *Txnrd1*, *Prdx1*, *Gclc*, *Sod1*, *Fth1*, and *Ephx1*, were also upregulated by DC-PGKI in LPS treated and untreated conditions, compared to the vehicle control (Fig. 5E−H and Figs. S5C−D). Consistently, the NRF2-dependent luciferase reporter assay in 293T cells also indicated that DC-PGKI could activate NRF2 (Fig. 5D). The same effect also detected in the BMDM cell line (Fig. S5E). Furthermore, two KEAP1 mutant/deficiency cancer cell lines treated with DC-PGKI have no effect on NRF2 accumulation (Fig. S5F), indicating the specificity of DC-PGKI. To better assess effect of DC-PGKI on NRF2, we carried out the NRF2 chromatin immunoprecipitation (CHIP)-qPCR assay. DC-PGKI treated resulted in a higher NRF2-binding signal to the proximity of *Il-1β*, *Il-6*, and *Nqo1* genes than the vehicle-treated group (Fig. 6I−K). Thromboxane synthase gene (*Txs*) intron, which is the negative control, remains the same. Collectively, these data suggest that anti-inflammation mechanism of DC-PGKI is dependent on activation of NRF2.

3.6. DC-PGKI alleviates DSS-induce mouse colitis

We next evaluated pharmacokinetic properties of DC-PGKI *in vivo*. DC-PGKI possessed a C_{max} of 38 ng/mL and an AUC of 253 h ng/mL, and exhibited low oral bioavailability of 11.2% (Supporting Information Fig. S6A−B). However, DC-PGKI had a favorable half-life (iv: 4.35 h, *po*: 5.29 h, Supporting Information Table S3). To determine whether DC-PGKI has the potential in inflammatory induced disease treatment. We evaluate the DC-PGKI therapeutic effect on DSS-induced acute colitis mice model. 5-Aminosalicylic acid (5-ASA), the standard treatment drug for ulcerative colitis, was included in our assay. The body weight of mice in DSS, DSS+5-ASA and DSS + DC-PGKI groups started to decrease on Day 4 and showed a great dropped

on Day 7, compared to the normal control. However, treatment of DC-PGKI significantly reduces body weight loss compared to DSS and DSS-5ASA groups (Fig. 6A). Consistently, the disease activity index (DAI) of the DC-PGKI treatment group decreases compared to the DSS group (Fig. 6B). The appearance of colon tissues and the shortening colon length caused by DSS is ameliorated by DC-PGKI treatment (Fig. 6C and D). H&E staining of colon tissues shows destructed musical structure, severe damage in crypts, and increased lymphocytes infiltration, while treatment of DC-PGKI, these effects are significantly attenuated (Fig. 6E and F). The pro-inflammatory cytokines level (IL-1β, IL-6) in serum (Fig. 6G and H) and tissue (Fig. 6I and J) were significantly reduced by DC-PGKI treatment compared to the DSS group, which is consistent with the *in vitro* effects.

To get insight into whether DC-PGKI could engage in PGK1 and activate NRF2 expression *in vivo*, we examine the change of KEAP1-NRF2 pathway in mice tissue. DSS injury mice show decreased NRF2 expression while co-treatment with DC-PGKI rescued the protein level of NRF2 (Fig. 6K), indicating the *in vivo* PGK1 engagement of DC-PGKI. Collectively, this data suggested that DC-PGKI is a potential therapeutic candidate agent for inflammatory diseases.

4. Discussion

Glycolysis is essential in cell energy generation and is the fundamental basis of biosynthesis. Aerobic glycolysis is identified to be the hallmark of malignant cell metabolism[2]. The normal cells, especially the immune cells, show the same phenomenon as cancer cells[5,7,10,59]. Glycolytic metabolite enzymes have been well-study in the highly glycolytic tumor and the activated immune cells. Many glycolytic enzymes have been characterized as the moonlighting protein, which possess other functions to correlate different biological activities with metabolism. Typically, the GAPDH[10,60], PKM2[13,54], and PGK1[32,36,37] are three multifunction metabolic enzymes. A lot of data have indicated that PGK1 is overexpressed in many tumors and confer chemotherapy resistance[23]. Many reports suggest that PGK1 has intermitted correlation to heat or oxygen stress resistance[37], implicating that PGK1 possesses other functions. However, small molecules targeting PGK1 are still scanty. The chemical probe represents either a powerful tool to explore the function of target or the starting point for drug development. Thus, we aim to discover more potential small molecules that inhibits PGK1 activity.

Intriguingly, DC-PGKI limits pro-inflammatory cytokines production in the LPS-primed macrophage. Also, DC-PGKI exhibits protection effects on DSS-induce acute colitis mice model. The gene manipulations assay demonstrates that the anti-inflammation effect of DC-PGKI is indeed dependent on PGK1, and unveils the new function of PGK1 in the innate system. Mechanically, DC-PGKI activates the KEAP-NRF2 pathway by inhibiting PGK1, and the accumulated NRF2 protein activates NRF2-downstream target genes' expression through the KEAP-NRF2 pathway. While the NRF2-Chip qPCR assay demonstrates that the DC-PGKI treatment restricts both *Il-1β* and *Il-6* genes' expression by increasing the NRF2 binding to the proximity of *Il-1β* and *Il-6* genes and hindering the recruitment of RNA Pol II.

The infiltrated-macrophage-derived IL-6 promotes tumorigenesis and supports the tumor cell's glycolysis by phosphorylating PGK1 in the tumor microenvironment of human glioblastoma
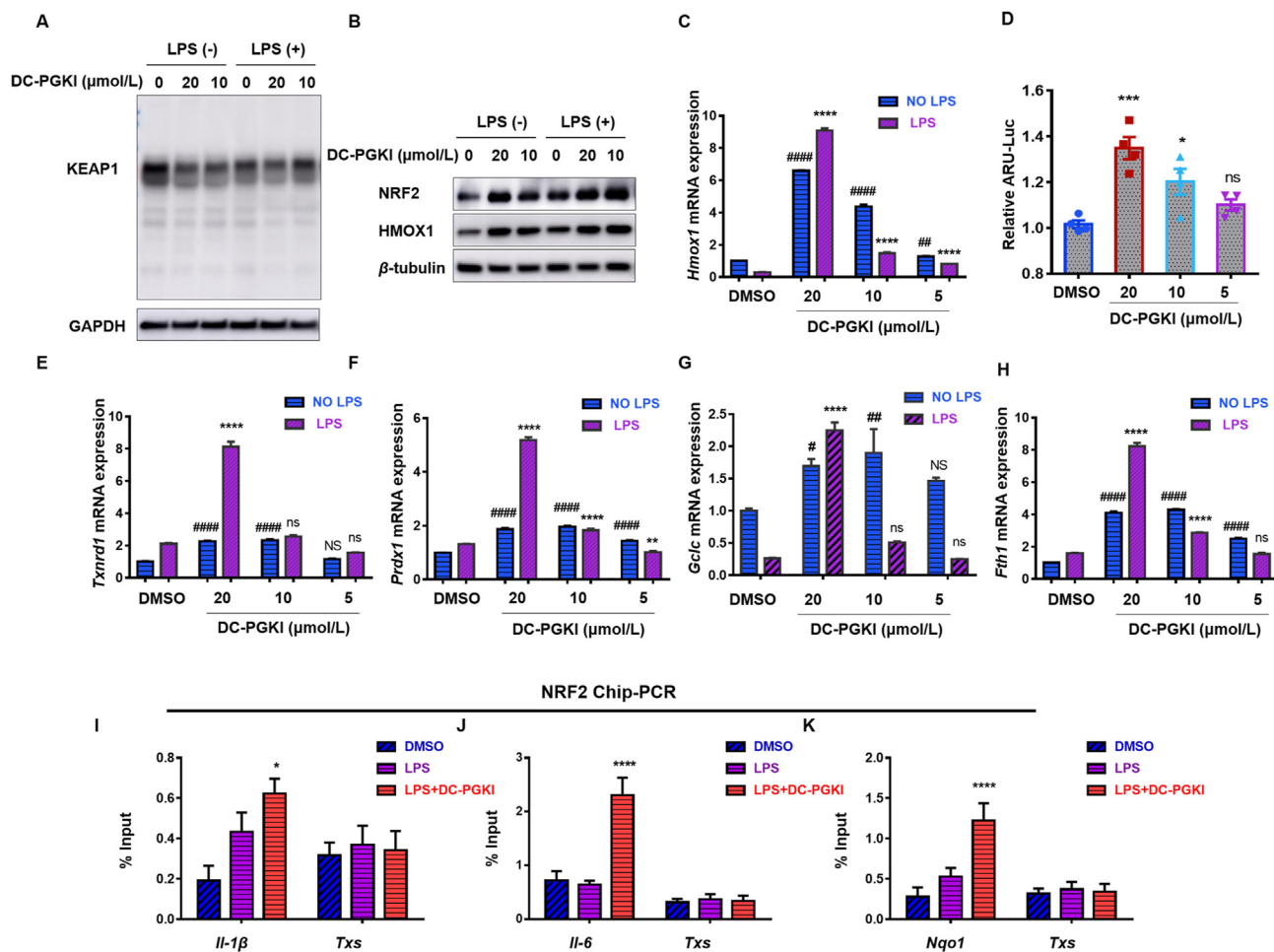
Figure 5 DC-PGKI promotes NRF2 accumulation to suppress IL-1β and IL-6 production. (A) DC-PGKI decreased KEAP1 protein level in RAW264.7 cells in the presence or absence of LPS-primed. (B) NRF2 was accumulated either with or without LPS-primed macrophage. DC-PGKI also increases the NRF2 downstream target gene HMOX1 mRNA level as well as protein level (C). (D) NRF2-dependent ARE reporter assay in 293T showed DC-PGKI could promote NRF2 binding to the ARE element. (E−H) The NRF2 downstream target genes transcription has been activated by DC-PGKI either in the rest or activate RAW264.7 cells. *Txnrd1*: thioredoxin reductase (E); *Prdx1*: peroxiredoxin 1 (F); *Gclc*: glutamate-cysteine ligase catalytic subunit (G); *Fth1*: ferritin heavy chain 1 (H). (I−K) NRF2 chromatin immunoprecipitation (CHIP)-qPCR assay indicated that DC-PGKI could enhance the binding of NRF2 to the proximal region of *Il-1β* (I), *Il-6* (J) genes. Error bar shows as mean ± SEM ($n = 3$). Statistical significance was defined as $*P < 0.05$, $**P < 0.01$, $***P < 0.001$, $****P < 0.0001$ by unpaired two-tailed Student's t-test by compared to the LPS-stimulated vehicle control group. While $^{\#}P < 0.05$, $^{\#\#}P < 0.01$, $^{\#\#\#}P < 0.001$, $^{\#\#\#\#}P < 0.0001$ were defined as Student's t-test by compared to the no LPS-stimulated vehicle control group.

multiform (GBM), and inhibition of PGK1 T243 phosphorylation or neutralization of IL-6 could inhibit tumor cell proliferation and tumorigenesis[34]. Our discovery shows that DC-PGKI could repress IL-6 expression in the macrophage by inhibiting PGK1, which means that DC-PGKI or other PGK1 inhibitors could serve as an anti-tumor agent. However, many post-transcriptional modifications of PGK1 have been reported to promote tumorigenesis in many tumors. DC-PGKI may show inconsistent potential in those modifications. We marked all the modified residues in the PGK1 activated-catalytic crystal structure (PDB: 2WZD), intriguingly, we found that all modifications occur in the C-terminal domain of PGK1, which is responsible for ADP/ATP binding (Supporting Information Fig. S7). Among those modifications, only K220 formed two hydrogen bonds with ADP, and acetylated K220 blocked ADP binding. The remaining modifications are far from the ADP/ATP pocket and have no direct interaction with ADP. Based on the fact that DC-PGKI is a competitor

of ADP/ATP, which is means that the higher binding affinity of ADP/ATP, the lower the potency of DC-PGKI. Thus, the acetylated K323 and K388, phosphorylated S203 and Y324, and *O*-GlcNAcylated T255 activate PGK1 though enhancing the binding affinity ADP/ATP, which may be resistant to DC-PGKI. For the phosphorylation on S256 and T243, which do not influence ADP/ATP binding affinity, DC-PGKI may show the same inhibitory effect as the WT PGK1. Accordingly, PGK1 has been reported to be overexpression in the synovial tissues and blood of human rheumatoid arthritis, which has overexpressed of several cytokines (IL-1β, IL-6, and IFN-γ)[61], and knockdown PGK1 results in decline IL-1β and IFN-γ production[62]. Hence, DC-PGKI may have a positive effect on rheumatoid arthritis treatment. However, all the applications should be careful consideration with sufficient scientific research.

In conclusion, we report DC-PGKI, a new scaffold inhibitor of PGK1, unveil that PGK1 is a regulator of proinflammatory
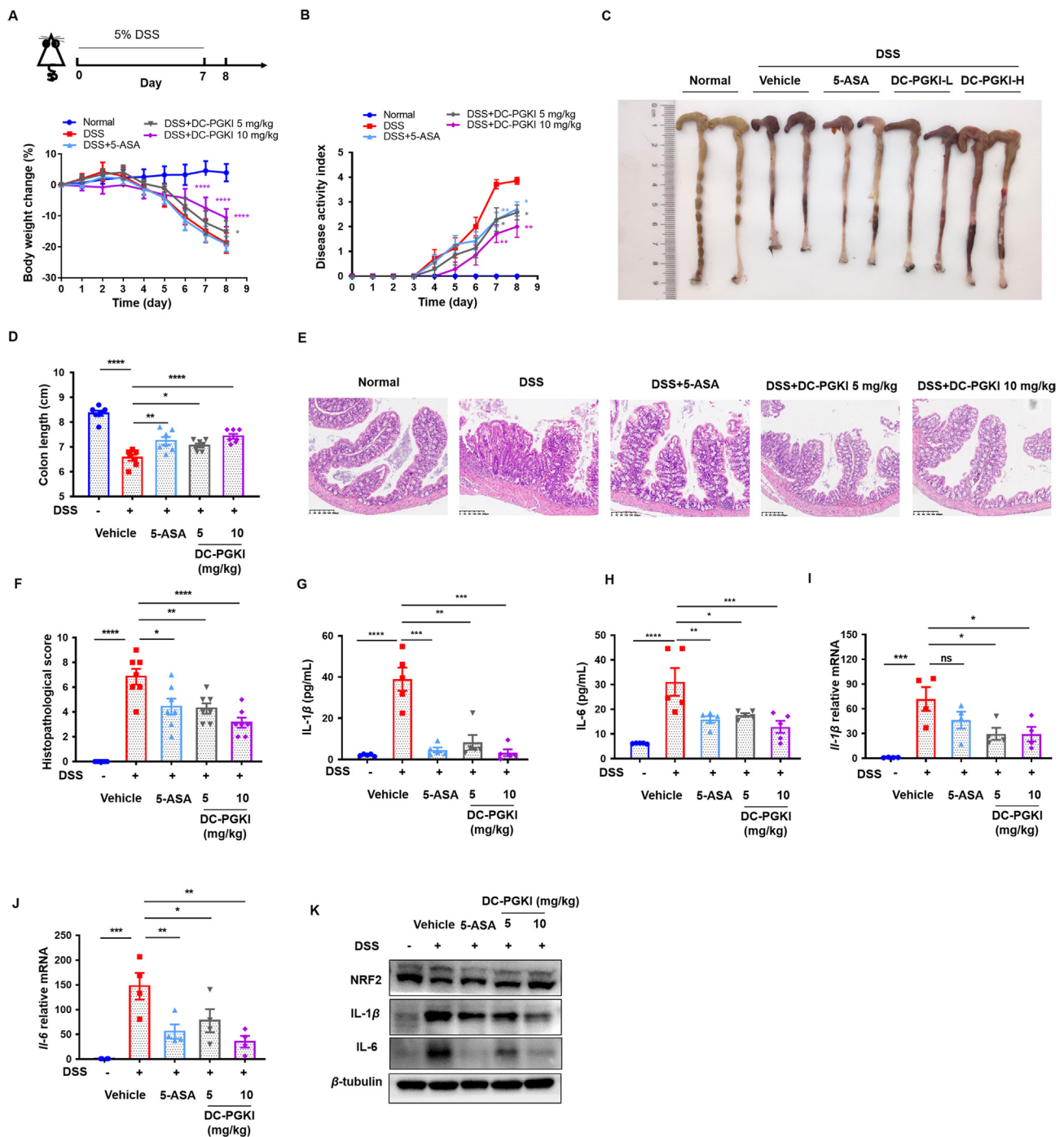
Figure 6 DC-PGKI alleviates DSS-induced colitis. (A) Body weight Change of mice subjected to colitis induction with 5% DSS treatment for 7 days, followed by drinking water for 1 day ($n = 7$). (B) Disease activity index (DAI) in each group ($n = 7$). (C) The appearance of colon tissues and (D) colon length of different groups ($n = 7$). (E) H&E staining of colon tissues. (F) Histopathological scores of mouse colon tissues in each group ($n = 7$). IL-1β (G) and IL-6 (H) serum levels of mice in each group were determined by the ELISA assay ($n = 5$). (I) and (J) The mRNA levels of Il-1β (I) and Il-6 (J) in mouse colon tissues of each group ($n = 4$). (K) The NRF2, IL-1β and IL-6 protein level in mouse colon tissues of each group. Weight changes are compared by two-way ANOVA. DAI scores are compared by Mann−Whitney U test. Other data are compared by unpaired two-tailed Student's t-test. Statistical significance is defined as *$P < 0.05$, **$P < 0.01$, ***$P < 0.001$, ****$P < 0.0001$ by unpaired two-tailed Student's t-test by compared to the DSS group.

cytokine production in LPS-challenged macrophages. Mechanistically, inhibition of PGK1 by DC-PGKI increases NRF2 accumulation, and the binding of NRF2 to the proximity of Il-1β and Il-6 genes, thereby inhibiting the production of Il-1β and Il-6.

Furthermore, DC-PGKI ameliorates mouse colitis induced by DSS. Thus, DC-PGKI may serve as a potential candidate for the treatment of inflammatory diseases, such as inflammatory bowel disease.

5. Conclusions

Here, we develop a high-throughput assay to screen novel PGK1 inhibitors and report a novel chemical scaffold inhibitor of PGK1 with $K_d = 99.08$ nmol/L, which suppresses pro-inflammatory cytokines production. DC-PGKI reveals the inhibition of PGK1 suppresses the production of IL-1β and IL-6 through NRF2 accumulation, which translocates to the nucleus then bind to the proximity of *Il-1β* and *Il-6* genes. The results from DSS induced colitis mouse model indicate that DC-PGKI effectively alleviates symptoms and pathological changes of colitis. These data suggest that DC-PGKI can serve as a probe to study novel function of PGK1 and also a therapeutic candidate agent for inflammatory disease.

Acknowledgments

Author contributions

Cheng Luo conceived the project. Cheng Luo provided intellectual contributions with Xiaoyan Shen. Liping Liao, Wenzhen Dang and Tingting Lin conceived and designed experiments, performed and analyzed experiments, and wrote the manuscript. Bing Zhou provided expert advice of Compound modification. Rong Fu, Jing Huang, Lei Feng, and Hongru Tao provided advice of high-throughput assay. Liping Liu and Mingchen Wang provided advice of enzymology. Senhao Xiao, Wen Li, and Jiacheng Li provided help of protein expression. Xingxing Diao, Jinghua Yu and Tonghai Liu provided help of the animal experiment. Kaixian Chen and Hualiang Jiang read the manuscript and provided suggestion about the paper. All authors discussed the manuscript.

Conflicts of interest

The authors declare no competing interests.

Appendix A. Supporting information

Supporting data to this article can be found online at https://doi.org/10.1016/j.apsb.2022.05.012.

References

1. Warburg O. On respiratory impairment in cancer cells. *Science* 1956;**124**:269−70.
2. Pavlova NN, Thompson CB. The emerging hallmarks of cancer metabolism. *Cell Metabol* 2016;**23**:27−47.
3. Wei Q, Qian Y, Yu J, Wong CC. Metabolic rewiring in the promotion of cancer metastasis: mechanisms and therapeutic implications. *Oncogene* 2020;**39**:6139−56.
4. Wenes M, Shang M, Di Matteo M, Goveia J, Martin-Perez R, Serneels J, et al. Macrophage metabolism controls tumor blood vessel morphogenesis and metastasis. *Cell Metabol* 2016;**24**:701−15.
5. Gerriets VA, Kishton RJ, Nichols AG, Macintyre AN, Inoue M, Ilkayeva O, et al. Metabolic programming and PDHK1 control CD4+ T cell subsets and inflammation. *J Clin Invest* 2015;**125**:194−207.
6. Peng M, Yin N, Chhangawala S, Xu K, Leslie CS, Li MO. Aerobic glycolysis promotes T helper 1 cell differentiation through an epigenetic mechanism. *Science* 2016;**354**:481−4.
7. Brand A, Singer K, Koehl GE, Kolitzus M, Schoenhammer G, Thiel A, et al. LDHA-associated lactic acid production blunts tumor immunosurveillance by T and NK cells. *Cell Metabol* 2016;**24**: 657−71.
8. Chesney JA, Telang S, Yaddanapudi K, Grewal JS. Targeting 6-phosphofructo-2-kinase (PFKFB3) as an immunotherapeutic strategy. *J Clin Oncol* 2016;**34**.
9. Millet P, Vachharajani V, McPhail L, Yoza B, McCall CE. GAPDH binding to TNF-alpha mRNA contributes to posttranscriptional repression in monocytes: a novel mechanism of communication between inflammation and metabolism. *J Immunol* 2016;**196**:2541−51.
10. Chang CH, Curtis JD, Maggi Jr LB, Faubert B, Villarino AV, O'Sullivan D, et al. Posttranscriptional control of T cell effector function by aerobic glycolysis. *Cell* 2013;**153**:1239−51.
11. Everts B, Amiel E, Huang SC, Smith AM, Chang CH, Lam WY, et al. TLR-driven early glycolytic reprogramming *via* the kinases TBK1-IKKε supports the anabolic demands of dendritic cell activation. *Nat Immunol* 2014;**15**:323−32.
12. Moon JS, Hisata S, Park MA, DeNicola GM, Ryter SW, Nakahira K, et al. mTORC1-induced HK1-dependent glycolysis regulates NLRP3 inflammasome activation. *Cell Rep* 2015;**12**:102−15.
13. Palsson-McDermott EM, Curtis AM, Goel G, Lauterbach MA, Sheedy FJ, Gleeson LE, et al. Pyruvate kinase M2 regulates Hif-1α activity and IL-1β induction and is a critical determinant of the warburg effect in LPS-activated macrophages. *Cell Metabol* 2015;**21**: 65−80.
14. Xie M, Yu Y, Kang R, Zhu S, Yang L, Zeng L, et al. PKM2-dependent glycolysis promotes NLRP3 and AIM2 inflammasome activation. *Nat Commun* 2016;**7**:13280.
15. Fu Q, Yu Z. Phosphoglycerate kinase 1 (PGK1) in cancer: a promising target for diagnosis and therapy. *Life Sci* 2020;**256**:117863.
16. Wu Y, Deng Y, Zhu J, Duan YC, Weng WW, Wu XHH. Pim 1 promotes cell proliferation and regulates glycolysis *via* interaction with MYC in ovarian cancer. *OncoTargets Ther* 2018;**11**:6647−56.
17. Zhang J, Zhang J, Wei Y, Li Q, Wang Q. ACTL6A regulates follicle-stimulating hormone-driven glycolysis in ovarian cancer cells *via* PGK1. *Cell Death Dis* 2019;**10**:811.
18. Shashni B, Sakharkar KR, Nagasaki Y, Sakharkar MK. Glycolytic enzymes PGK1 and PKM2 as novel transcriptional targets of PPAR-gamma in breast cancer pathophysiology. *J Drug Target* 2013;**21**: 161−74.
19. Jiang Y, He R, Jiang Y, Liu D, Tao L, Yang M, et al. Transcription factor NFAT5 contributes to the glycolytic phenotype rewiring and pancreatic cancer progression *via* transcription of PGK1. *Cell Death Dis* 2019;**10**:948.
20. Liang C, Shi S, Qin Y, Meng Q, Hua J, Hu Q, et al. Localisation of PGK1 determines metabolic phenotype to balance metastasis and proliferation in patients with SMAD4-negative pancreatic cancer. *Gut* 2020;**69**:888−900.
21. Ge J, Li J, Na S, Wang P, Zhao G, Zhang X. miR-548c-5p inhibits colorectal cancer cell proliferation by targeting PGK1. *J Cell Physiol* 2019;**234**:18872−8.
22. Zieker D, Konigsrainer I, Traub F, Nieselt K, Knapp B, Schillinger C, et al. PGK1 a potential marker for peritoneal dissemination in gastric cancer. *Cell Physiol Biochem* 2008;**21**:429−36.

23. Schneider CC, Archid R, Fischer N, Buhler S, Venturelli S, Berger A, et al. Metabolic alteration - overcoming therapy resistance in gastric cancer *via* PGK-1 inhibition in a combined therapy with standard chemotherapeutics. *Int J Surg* 2015;**22**:92−8.

24. Tang SW, Chang WH, Su YT, Chen YC, Lai YH, Wu PT, et al. MYC pathway is activated in clear cell renal cell carcinoma and essential for proliferation of clear cell renal cell carcinoma cells. *Cancer Lett* 2009; **273**:35−43.

25. Semenza GL. Targeting HIF-1 for cancer therapy. *Nat Rev Cancer* 2003;**3**:721−32.

26. Fu D, He C, Wei J, Zhang Z, Luo Y, Tan H, et al. PGK1 is a potential survival biomarker and invasion promoter by regulating the HIF-1alpha-mediated epithelial-mesenchymal transition process in breast cancer. *Cell Physiol Biochem* 2018;**51**:2434−44.

27. Wang R, Dillon CP, Shi LZ, Milasta S, Carter R, Finkelstein D, et al. The transcription factor Myc controls metabolic reprogramming upon T lymphocyte activation. *Immunity* 2011;**35**:871−82.

28. Wang S, Jiang B, Zhang T, Liu L, Wang Y, Wang Y, et al. Correction: insulin and mTOR pathway regulate HDAC3-mediated deacetylation and activation of PGK1. *PLoS Biol* 2015;**13**:e1002287.

29. Wang S, Jiang B, Zhang T, Liu L, Wang Y, Wang Y, et al. Insulin and mTOR pathway regulate HDAC3-mediated deacetylation and activation of PGK1. *PLoS Biol* 2015;**13**:e1002243.

30. Hu H, Zhu W, Qin J, Chen M, Gong L, Li L, et al. Acetylation of PGK1 promotes liver cancer cell proliferation and tumorigenesis. *Hepatology* 2017;**65**:515−28.

31. Qian X, Li X, Cai Q, Zhang C, Yu Q, Jiang Y, et al. Phosphoglycerate kinase 1 phosphorylates beclin1 to induce autophagy. *Mol Cell* 2017; **65**:917−31.e6.

32. Li X, Jiang Y, Meisenhelder J, Yang W, Hawke DH, Zheng Y, et al. Mitochondria-translocated PGK1 functions as a protein kinase to co-ordinate glycolysis and the TCA cycle in tumorigenesis. *Mol Cell* 2016;**61**:705−19.

33. Li X, Qian X, Jiang H, Xia Y, Zheng Y, Li J, et al. Nuclear PGK1 alleviates ADP-dependent inhibition of CDC7 to promote DNA replication. *Mol Cell* 2018;**72**:650−60.e8.

34. Zhang Y, Yu G, Chu H, Wang X, Xiong L, Cai G, et al. Macrophage-associated PGK1 phosphorylation promotes aerobic glycolysis and tumorigenesis. *Mol Cell* 2018;**71**:201−15.e7.

35. Qian X, Li X, Shi Z, Xia Y, Cai Q, Xu D, et al. PTEN suppresses glycolysis by dephosphorylating and inhibiting autophosphorylated PGK. *Mol Cell* 2019;**76**:516−27.e7.

36. Nie H, Ju H, Fan J, Shi X, Cheng Y, Cang X, et al. *O*-GlcNAcylation of PGK1 coordinates glycolysis and TCA cycle to promote tumor growth. *Nat Commun* 2020;**11**:36.

37. Chen X, Zhao C, Li X, Wang T, Li Y, Cao C, et al. Terazosin activates Pgk1 and Hsp90 to promote stress resistance. *Nat Chem Biol* 2015;**11**: 19−25.

38. Bollong MJ, Lee G, Coukos JS, Yun H, Zambaldo C, Chang JW, et al. A metabolite-derived protein modification integrates glycolysis with KEAP1−NRF2 signalling. *Nature* 2018;**562**:600−4.

39. Manicone AM, Birkland TP, Lin M, Betsuyaku T, van Rooijen N, Lohi J, et al. Epilysin (MMP-28) restrains early macrophage recruitment in *Pseudomonas aeruginosa* pneumonia. *J Immunol* 2009;**182**:3866−76.

40. Zhang JH, Chung TD, Oldenburg KR. A simple statistical parameter for use in evaluation and validation of high throughput screening assays. *J Biomol Screen* 1999;**4**:67−73.

41. Li F, Han M, Dai P, Xu W, He J, Tao X, et al. Distinct mechanisms for TMPRSS2 expression explain organ-specific inhibition of SARS-CoV-2 infection by enzalutamide. *Nat Commun* 2021;**12**:866.

42. Kobayashi EH, Suzuki T, Funayama R, Nagashima T, Hayashi M, Sekine H, et al. Nrf2 suppresses macrophage inflammatory response by blocking proinflammatory cytokine transcription. *Nat Commun* 2016;**7**:11624.

43. Weisser SB, Brugger HK, Voglmaier NS, McLarren KW, van Rooijen N, Sly LM. SHIP-deficient, alternatively activated macro-phages protect mice during DSS-induced colitis. *J Leukoc Biol* 2011; **90**:483−92.

44. Kim JJ, Shajib MS, Manocha MM, Khan WI. Investigating intestinal inflammation in DSS-induced model of IBD. *JoVE* 2012;**60**: e3678.

45. Harris RA. Glycolysis overview. *Encycl Biol Chem* 2013:443−7.

46. Varga A, Lionne C, Lallemand P, Szabo J, Adamek N, Valentin C, et al. Direct kinetic evidence that lysine 215 is involved in the phospho-transfer step of human 3-phosphoglycerate kinase. *Biochemistry* 2009;**48**:6998−7008.

47. Li W, Liao LP, Song N, Liu YJ, Ding YL, Zhang YY, et al. Natural product 1,2,3,4,6-penta-*O*-galloyl-*β*-D-glucopyranose is a reversible inhibitor of glyceraldehyde 3-phosphate dehydrogenase. *Acta Pharmacol Sin* 2022;**43**:470−82.

48. Wang WL, Jiang ZR, Hu C, Chen C, Hu ZQ, Wang AL, et al. Pharmacologically inhibiting phosphoglycerate kinase 1 for glioma with NG52. *Acta Pharmacol Sin* 2021;**42**:633−40.

49. Vitale I, Manic G, Coussens LM, Kroemer G, Galluzzi L. Macro-phages and metabolism in the tumor microenvironment. *Cell Metabol* 2019;**30**:36−50.

50. Palsson-McDermott EM, O'Neill LAJ. Targeting immunometabolism as an anti-inflammatory strategy. *Cell Res* 2020;**30**:300−14.

51. Jacobs SR, Herman CE, Maciver NJ, Wofford JA, Wieman HL, Hammen JJ, et al. Glucose uptake is limiting in T cell activation and requires CD28-mediated Akt-dependent and independent pathways. *J Immunol* 2008;**180**:4476−86.

52. Shirai T, Nazarewicz RR, Wallis BB, Yanes RE, Watanabe R, Hilhorst M, et al. The glycolytic enzyme PKM2 bridges metabolic and inflammatory dysfunction in coronary artery disease. *J Exp Med* 2016; **213**:337−54.

53. Vander Heiden MG, Christofk HR, Schuman E, Subtelny AO, Sharfi H, Harlow EE, et al. Identification of small molecule inhibitors of pyruvate kinase M2. *Biochem Pharmacol* 2010;**79**:1118−24.

54. Angiari S, Runtsch MC, Sutton CE, Palsson-McDermott EM, Kelly B, Rana N, et al. Pharmacological activation of pyruvate kinase M2 Inhibits CD4+ T Cell pathogenicity and suppresses autoimmunity. *Cell Metabol* 2020;**31**:391−405.e8.

55. Tannahill GM, Curtis AM, Adamik J, Palsson-McDermott EM, McGettrick AF, Goel G, et al. Succinate is an inflammatory signal that induces IL-1beta through HIF-1alpha. *Nature* 2013;**496**: 238−42.

56. Kornberg MD, Bhargava P, Kim PM, Putluri V, Snowman AM, Putluri N, et al. Dimethyl fumarate targets GAPDH and aerobic glycolysis to modulate immunity. *Immunity* 2018;**360**:449−53.

57. Lampropoulou V, Sergushichev A, Bambouskova M, Nair S, Vincent EE, Loginicheva E, et al. Itaconate links inhibition of succinate dehydrogenase with macrophage metabolic remodeling and regulation of inflammation. *Cell Metabol* 2016;**24**:158−66.

58. Mills EL, Ryan DG, Prag HA, Dikovskaya D, Menon D, Zaslona Z, et al. Itaconate is an anti-inflammatory metabolite that activates Nrf2 *via* alkylation of KEAP1. *Nature* 2018;**556**:113−7.

59. Krawczyk CM, Holowka T, Sun J, Blagih J, Amiel E, DeBerardinis RJ, et al. Toll-like receptor-induced changes in glycolytic metabolism regulate dendritic cell activation. *Blood* 2010;**115**:4742−9.

60. Galván-Peña S, Carroll RG, Newman C, Hinchy EC, Palsson-McDermott E, Robinson EK, et al. Malonylation of GAPDH is an inflammatory signal in macrophages. *Nat Commun* 2019;**10**:338.

61. Alghasham A, Rasheed Z. Therapeutic targets for rheumatoid arthritis: progress and promises. *Autoimmunity* 2014;**47**:77−94.

62. Zhao Y, Yan X, Li X, Zheng Y, Li S, Chang X. PGK1, a glucose metabolism enzyme, may play an important role in rheumatoid arthritis. *Inflamm Res* 2016;**65**:815−25.